Eur Radiol (2006) 16: 2334–2340
DOI 10.1007/s00330-006-0217-2

J. Geleijns
M. Salvadó Artells
W. J. H. Veldkamp
M. López Tortosa
A. Calzado Cantera

Quantitative assessment of selective in-plane shielding of tissues in computed tomography through evaluation of absorbed dose and image quality

Received: 16 August 2005
Revised: 26 January 2006
Accepted: 27 February 2006
Published online: 8 April 2006

J. Geleijns (✉) · W. J. H. Veldkamp
Radiology Department,
Leiden University Medical Center,
Albinusdreef 2,
2333 ZA Leiden, The Netherlands
e-mail: K.Geleijns@lumc.nl
Tel.: +31-71-5262049
Fax: +31-71-5248256

M. Salvadó Artells · M. López Tortosa
Departament de Ciències Mèdiques
Bàsiques, Universitat Rovira i Virgili,
Facultat de Medicina i Ciències de la Salut,
C/ Sant Llorenç 21,
43201 Reus, Tarragona, Spain

A. Calzado Cantera
Departamento de Radiología,
Universidad Complutense de Madrid,
28040 Madrid, Spain

Abstract This study aimed at assessment of efficacy of selective in-plane shielding in adults by quantitative evaluation of the achieved dose reduction and image quality. Commercially available accessories for in-plane shielding of the eye lens, thyroid and breast, and an anthropomorphic phantom were used for the evaluation of absorbed dose and image quality. Organ dose and total energy imparted were assessed by means of a Monte Carlo technique taking into account tube voltage, tube current, and scanner type. Image quality was quantified as noise in soft tissue. Application of the lens shield reduced dose to the lens by 27% and to the brain by 1%. The thyroid shield reduced thyroid dose by 26%; the breast shield reduced dose to the breasts by 30% and to the lungs by 15%. Total energy imparted (unshielded/shielded) was 88/86 mJ for computed tomography (CT) brain, 64/60 mJ for CT cervical spine, and 289/260 mJ for CT chest scanning. An increase in image noise could be observed in the ranges were bismuth shielding was applied. The observed reduction of organ dose and total energy imparted could be achieved more efficiently by a reduction of tube current. The application of in-plane selective shielding is therefore discouraged.

Keywords X-ray computed tomography · Radiation protection · Radiation effects

Introduction

With the evolution of computed tomography (CT) toward a versatile and fast technique for three-dimensional (3D) imaging, the variety of clinical applications and consequently the number of annually performed clinical CT examinations has seen rapid growth. At the same time, consciousness and concern about radiation exposure of patients has increased. Various measures and technologies for radiation protection have been recommended, including shielding of organs either outside [1, 2] or inside the scan range [3].

Absorbed dose to superficial organs and tissues was reported to be reduced by applying a sheet consisting of a compound of latex and bismuth on the skin close to superficial organs and tissues within the scan range, i.e., close to the eye lens during CT brain scans [4–9], the thyroid during CT cervical spine [5] and CT chest scans [7, 8], and breasts during CT chest scans [3, 5, 7]. Dosimetry was generally performed with thermoluminescence dosimeters (TLD) but also film [4], solid-state [10], and Monte Carlo dosimetry [9] were applied. In adults, a dose reduction to the eye lens was reported to be about 40–50% [4–7], to the thyroid 57–67% [5, 7, 8], and to the breasts 51–52% [5, 7]. For pediatric chest CT, a 29% reduction in the breast dose and for pediatric brain CT, a 30–40% reduction in eye-lens dose was reported [3, 9].

Assessment of image quality was in general performed in qualitative terms. Deterioration of image quality by beam-hardening artefacts was identified as streaks, especially close to the shield, but they were reported not to extend to the tissues of interest for diagnosis, e.g., lung

parenchyma [5] or brain [6]. In pediatric CT of the chest, no artefacts in the breast or lung tissue were recognized [3], and no obvious change in image quality resulted from eye-lens shielding in cranial CT [9, 10]. The artefact produced by thyroid shielding was reported as slightly distracting but did not interfere with interpretation of the images [8]. Artefacts projected in the brain were reported due to wrinkled eye-lens shields. One publication described that shields affect Hounsfield units (HU), thus falsifying quantitative information [4]. It was reported that no increased noise was observed in the lung parenchyma or mediastinum [5], and no statistically significant difference in noise was observed in the lungs [3].

Limitations of published reports are that dose assessment in adults was restricted to measurements with TLD, film, or a solid-state detector attached to the skin whereas results were interpreted as organ and tissue doses. However, direct assessment of organ and tissue doses is preferred. Furthermore, in addition to organ dose, a generic measure of patient exposure should also be provided, such as total energy imparted. Papers published so far have not provided quantitative information on the impact of selective shielding on image quality. In radiation protection, the delicate balance between image quality and patient dose can only be established if both of these two aspects are assessed quantitatively.

Materials and methods

Shields and anthropomorphic phantom

Shields for in-plane shielding are available under the name AttenuRad radioprotective garments (F&L Medical Products Co., Vandergrift, PA, USA). They consist of thin, flexible latex sheets containing 3.4 $g.cm^{-2}$ of bismuth. The eye-lens shield measures 14×3.5 cm^2, the thyroid shield 15×8.5 cm^2, and each of the sheets forming the pair of breast shields measures 20×25 cm^2. Edges of the shields are rounded and designed to accurately fit the shape of the body.

An anthropomorphic Rando phantom (Phantom Laboratory, Salem, NY, USA) representing the skull and trunk of a 175-cm tall male weighting 73.5 kg was manufactured on demand in one piece to study the effect of selective shielding on image quality and absorbed dose. The phantom is composed of synthetic materials representing the density and X-ray attenuation of lung tissue and soft tissue and includes a human skeleton [11]. Two breasts modules composed of tissue-equivalent material (bees wax) of 260 cm^3 each could be added to the phantom.

Multislice CT scans, acquisition and reconstruction

For the purpose of dose calculations and assessment of image quality, multislice CT (MSCT) scans of the phantom were obtained at an Aquilion16CFX scanner (Toshiba, Japan) (120 kVp, 16×1 mm, 100 mAs). The scan field of view (SFOV) was 400 mm. A total of 259 images were reconstructed as 4-mm thick contiguous slices covering the entire phantom. The reconstructed field of view was 400 mm, and a 512^2 image matrix was used. Scans were made of five different configurations; each scan was repeated twice in order to enhance the accuracy of noise assessment. The selected scan configurations included two acquisitions without shielding, i.e., respectively with and without the breast modules, and three configurations with shielding, i.e., respectively with the eye-lens shield, the thyroid shield, and the breast shield.

Dosimetry

For dosimetry purposes, voxel phantoms were derived from the CT scans of the anthropomorphic phantom. Original axial images were reduced to 256×256 pixels; corresponding voxels measured 1.6×1.6×4 mm^3. The location of the eye lens and thyroid within the voxel phantom were established by a radiologist (AS). Breast tissue and lung tissue could be easily distinguished.

Dosimetry was performed with a Monte Carlo computer program based on the EGS4 code [12, 13]. The EGS4 code is able to simulate transport of photons with energies of 1 keV and higher and electrons with energies of 10 keV and higher. In this study, a cutoff energy for photons of 5 keV and for electrons of 30 keV was used. The cutoff implies that electrons and photons with lower energies are assumed to disseminate their energy locally. The Monte Carlo computer program was designed to yield the dose distribution within the anthropomorphic phantom. Special attention was paid to simulation of the X-ray beam, taking into account spectral characteristics of the X-ray beam, the effect of beam shaping filters, and penumbra effects caused by the focus and collimator. Two beam-shaping filters were simulated, a “head” beam shaping filter for the CT brain and the CT cervical spine scan and a “body” beam shaping filter for the CT chest scan. For each simulated 360° rotation of the X ray beam 3×10^6 photon histories were included in the Monte Carlo simulation, which corresponds to approximately 5 mi calculation time. The discreet increment of the angular position of the focus is sufficiently small ($\sim1.2\times10^{-4}$°) to simulate a continuous helical acquisition. Validation of the Monte Carlo simulation program was achieved prior to this study by comparing calculated doses with dose measurements, which resulted in differences that were smaller than 7% [14]. For this study, an additional validation of the Monte Carlo computer program for acquisitions with the Toshiba Aquilion 16CFX scanner was achieved by comparing measured and calculated CT dose index free in air ($CTDI_{air}$) and weighted CTDI ($CTDI_w$).

Measurements of the transmission of the bismuth shields were performed using an X-ray beam with a half-value layer of 8.1 mm aluminum. Voxelized bismuth shields, composed of a compound of latex and bismuth, were then designed to accurately reproduce the measured attenuation.

Finally, Monte Carlo simulations of dose distribution within the anthropomorphic phantom were performed for a scanned range of 18.4 cm for the CT brain scan, 15.6 cm for the cervical spine scan, and 33.6 cm for the chest scan; the simulated SFOV was 240 mm for CT brain and cervical spine and 400 mm for CT chest. For the percentage of dose reduction in organs and tissues, a generalized acquisition protocol was assumed (120 kVp, 16×1 mm, 100 mAs, pitch factor 1). Separate simulations were performed both with and without bismuth shielding. The simulations yielded unshielded and shielded organ and tissue doses (eye lens, brain, thyroid, breast, lungs). Although bismuth shielding aims at a selective reduction of organ dose, an evaluation of bismuth shielding on total energy imparted is also warranted since stochastic radiation risks are primarily correlated to such a generic measure of patient exposure. Thus, unshielded and shielded total energy imparted to the anthropomorphic phantom was assessed. In addition, organ dose and tissue equivalent dose was calculated for actual acquisition protocols in clinical use at our institute (120 kV, 16×1 mm; brain scan at 200 mAs, FOV 240 mm, pitch factor 0.94; neck scan 65 mAs, FOV 240 mm, pitch factor 1.44; chest scan 70 mAs, FOV 400 mm, pitch factor 1.44).

Image quality

Bismuth shields generate image artefacts (beam-hardening artefacts causing streaks, blooming, and a shift in HU) that are hard to quantify. Shielding is also expected to cause an increase of image noise, which can be easily quantified. Image noise is a key indicator of image quality since it limits the visualization of low-contrast lesions. Effects of shielding on noise, once quantified, can be correlated to tube current–rotation time product (mAs).

The most obvious approach for noise measurement seems to be subtraction of subsequent acquisitions. However, this was not feasible since axial image subtraction not only revealed image noise but also artefacts such as helical and interpolation artefacts. This is probably attributable to the random projection angle at the start of each acquisition [15]. Noise measurements were restricted to the homogeneous soft tissue simulating parts of the phantom since substantial structured noise was present within bone, simulated lung tissue, and breast modules. A measure of image noise was derived by image processing (MatLab, MathWorks Inc., Novi, MI, USA). First, a segmentation of soft tissue within the images of the anthropomorphic phantom was performed by selecting all pixels with HU within a predefined window (window width 100′ window level 20). This segmentation was followed by an erosion of segmented soft tissue using a disk-shaped structuring element with a diameter of nine pixels. Next, a new window level was defined by determining the mean HU of the segmented pixels, and the segmentation procedure was repeated with the new window level and the same window width as in the first segmentation. Each image was subdivided in square regions of interest (ROIs), each measuring 8×8 pixels. Only square regions that were entirely located within the segmented regions were taken into account. For each ROI, image noise was calculated as the standard deviation of HU. Image noise was expressed for each image as the median value of the standard deviations measured within the ROI's, thus reducing the influence of outliers, e.g., caused by beam-hardening artefacts.

In CT, a linear relationship is expected under quantum limited conditions between the inverse square of the noise ($1/\sigma^2$) and tube charge (mAs). For each 4-mm thick slice of the anthropomorphic phantom, a linear regression of these two parameters was established experimentally for tube current–rotation time products ranging from 40 to 100 mAs, enabling accurate assessment of the increase in image noise when lowering the tube current in unshielded acquisitions.

Table 1 Comparison of measured and calculated $CTDI_{air}$ and $CTDI_w$ (mGy/100 mAs) for validation of the Monte Carlo simulations for the Aquilion CFX16 CT scanner operating at four different tube voltages and for two beam shaping filters (head and body)

Tube	Head configuration				Body configuration			
Voltage	$CTDI_{air}$		$CTDI_w$		$CTDI_{air}$		$CTDI_w$	
kVp	(mGy/100 mAs)		(mGy/100 mAs)		(mGy/100 mAs)		(mGy/100 mAs)	
	Measured	Calculated	Measured	Calculated	Measured	Calculated	Measured	Calculated
80	13.0	12.5	7.2	7.0	20.6	20.1	4.3	4.5
100	20.8	20.4	12.7	12.5	30.0	29.6	7.5	7.6
120	27.6	28.9	19.0	19.0	40.3	40.7	11.0	11.3
135	38.3	39.4	24.4	25.1	48.1	48.2	14.8	14.3

Head and body configuration refers to the beam shaping filters and the CT dose phantoms
$CTDI_{air}$ computed tomography dose index free in air, *$CTDI_w$* weighted computed tomography dose index

Results

Dosimetry

For validation of the Monte Carlo computer program, the $CTDI_{air}$ and $CTDI_{w}$ were measured and calculated. Results are presented in Table 1. The average deviation of the calculated dose values compared eith the measured values was only 0.1%, ranging between −3.8% and 4.7%. This confirms good performance of the Monte Carlo technique and adequate simulation of the dose distribution within the cylindrical phantoms. Measured transmission of X-rays through the simulated bismuth shield (53±3%) was similar to the calculated transmission (51±3%), confirming sufficient accurate simulation of the shielding.

Subsequently, organ and tissue doses and total energy imparted were calculated. Application of the eye-lens shield reduced the dose to the eye lens by 27% and the dose to the brain by 1%. The thyroid shield reduced thyroid dose by 26%. The breast shield reduced dose to the breasts by 30% and dose to the lungs by 15%. Total energy imparted to the anthropomorphic phantom was 88 mJ (unshielded) and 86 mJ (shielded) for the CT brain, 64 mJ (unshielded) and 60 mJ (shielded) for the CT cervical spine, and 289 mJ (unshielded) and 260 mJ (shielded) for the CT chest scan. For clinical acquisition protocols, an equivalent dose for the eye

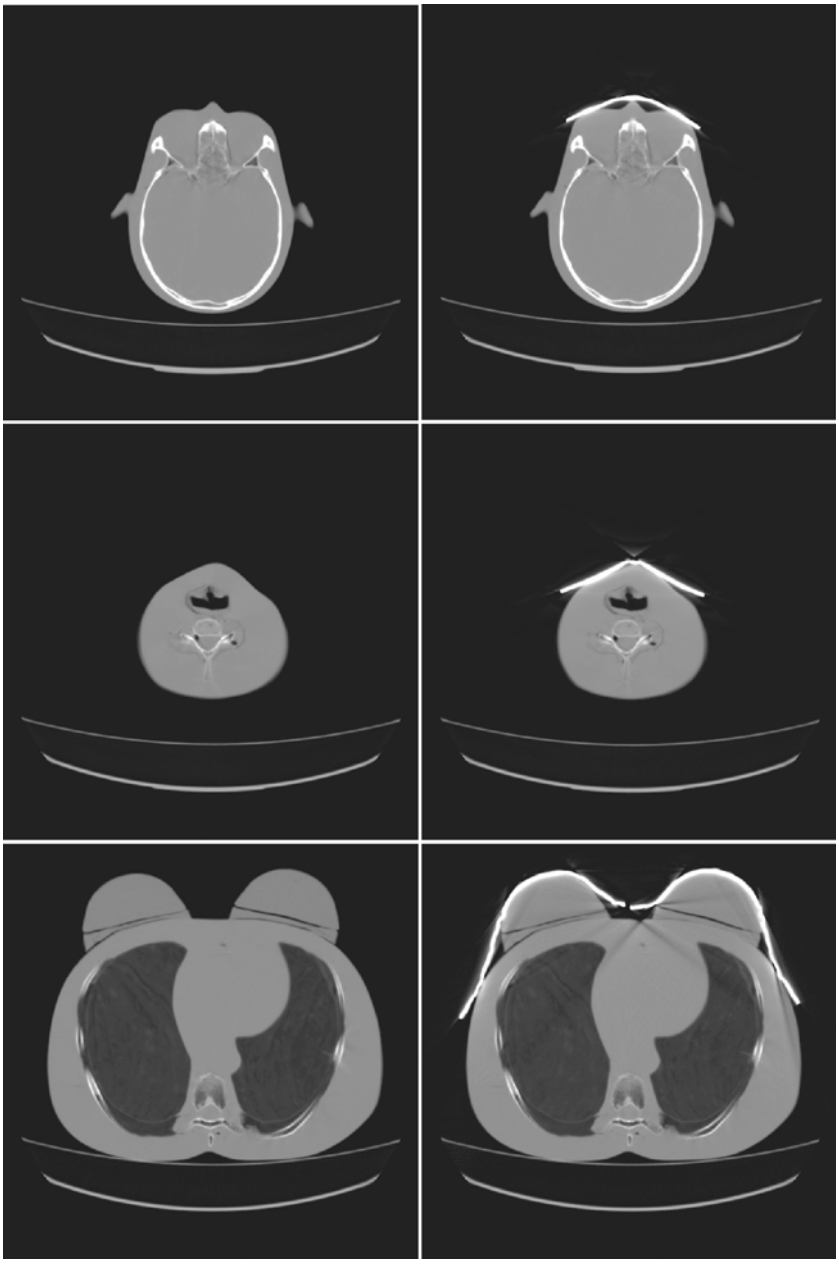

Fig. 1 Images representing unshielded and shielded acquisitions from respectively a computed tomography (CT) brain, CT cervical spine, and CT chest scan

lens was 29.1 mSv (unshielded) and 21.8 mSv (shielded), for the brain 22.9 mSv (unshielded) and 22.6 mSv (shielded) (both brain scan), for the thyroid 9.4 mSv (unshielded) and 7.0 mSv (shielded) (neck scan), for the breasts 6.0 mSv (unshielded) and 4.2 mSv (shielded), for the lungs 6.7 mSv (unshielded) and 5.7 mSv (shielded) (both chest scan).

Image quality

Shielded images in Fig. 1 illustrate beam-hardening artefacts caused by bismuth shielding; they are most noticeable for the breast shield. Measurement of noise in the images demonstrated the expected increase of noise in images that were affected by shielding (Fig. 2). The increase of noise by the relatively small eye shield was only modest (Fig. 2a) whereas the increase in noise introduced by the thyroid shield and breast shield was more prominent (Fig. 2b). The increase in noise caused by the breast shield made noise in the shielded images dominant compared with adjacent images in the range of a typical chest scan. A subsequent evaluation aimed at translating a theoretical reduction of tube current and the associated proportional reduction in organ dose and total energy imparted into an

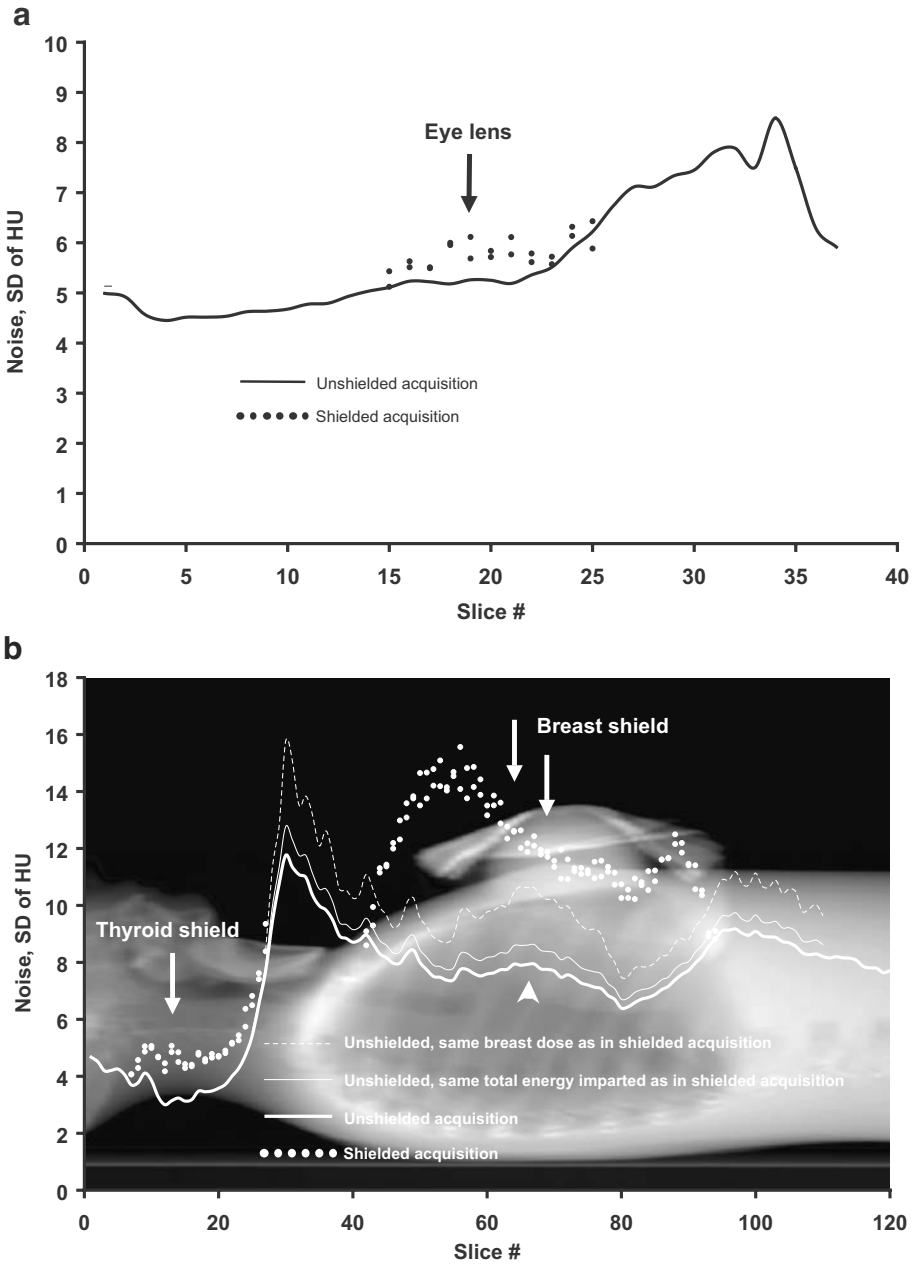

Fig. 2 Image noise measured with and without eye-lens shielding for the computed tomography (CT) brain scan. **a** *Arrow* indicates increased noise in shielded images (*closed dots*) and **b** noise with and without thyroid or breast shield for a CT chest scan. The *arrow* pointing at *closed dots* indicates increased noise due to thyroid shielding; the *two arrows* pointing at *closed dots* indicate increased noise due to breast shielding; the *single arrowhead* indicates the range of breast modules. The *thin line* in **b** corresponds with a 10.3% reduction of tube current and thus represents an acquisition yielding the same energy imparted as the shielded acquisition, showing a much lower noise level within the shielded range. The *thin dotted line* in **b** corresponds with a 30% reduction of tube current and thus represents an acquisition yielding the same breast dose as the shielded acquisition, showing a lower noise level within the shielded range. A sagittal reformat covering only part of the phantom and bismuth shields is shown in **b**

increase in noise within the unshielded images. To achieve this, a linear regression between tube charge and the inverse of the square noise was derived. A good correlation was found ($r_{average}$=0.985). A y-intercept larger than zero was found, indicating a substantial contribution of other sources of noise than quantum noise (e.g., equipment noise) at very low doses, i.e., doses well below the range considered in this study.

Bismuth shielding resulted in a slight reduction of total energy imparted to the anthropomorphic phantom for the CT brain (1.7%), CT cervical spine (5.8%), and CT chest (10.3%) scans. This reduction can, of course, also be achieved by an equal percentage decrease of tube current. This would cause a modest, almost unnoticeable, increase of image noise within the entire scanned range, an increase by less than 1% (CT brain), less than 3% (CT cervical spine), and about 5.5% (CT chest), respectively (Fig. 2b).

Discussion

Dose reduction by selective shielding should be reviewed in the context of the detriment that can be induced by radiation, i.e., deterministic effects (cataract applicable to the eye lens) and stochastic effects (tumor induction applicable to most tissues including brain, thyroid, breasts, and lung). Assessment of the efficacy of selective shielding must be based on a quantitative evaluation of absorbed dose and image quality.

Deterministic effects only occur when a certain threshold dose is exceeded. The generally accepted linear nonthreshold model for stochastic effects implies that even at low doses, a certain probability of tumor induction occurs; the probability increases proportionally with absorbed dose. The probability of occurrence of stochastic effects should be limited by keeping radiation exposure as low as reasonably achievable.

The threshold dose for radiation-induced cataract of 5 Sv (total dose equivalent received in a single exposure [16]) is not even approached in regular CT brain scans, even after repeated (multiphase) examinations or in intensive follow-up schemes assuming a typical dose equivalent to the eye lens during brain scanning of 30–60 Sv. Therefore, the 27% reduction of eye-lens dose achieved by selective shielding may be of minor importance for avoidance of radiation-induced cataract. The insignificant reduction of total energy imparted by the eye shield, knowingly 1.7%, can be achieved more efficiently, at least theoretically, by a 1.7% reduction of tube current. Image artefacts, costs, and the extra waste caused by the disposable eye shields are additional arguments against the application of the eye shields. It is considered good practice in sequential CT brain scanning to achieve substantial reduction of eye-lens dose by gantry tilting, thus keeping the eye lens just out of the X-ray beam. With current helical multislice acquisition techniques for CT brain scanning, tilting is not effective for dose reduction of the lens due to the effect of z-overranging [17].

The exposed thyroid is at risk of stochastic effects, and the thyroid shield reduces dose to the thyroid by 26% but corresponds to only a 5.8% reduction of the total energy imparted from a CT cervical spine scan. The modest reduction in total energy imparted by shielding is achieved at the cost of a measurable increase of noise in images within the shielded range and at the cost of mild but noticeable beam-hardening artefacts. Again, costs and extra waste are further arguments against the application of the disposable thyroid shield. An alternative, and more effective measure, for reducing total energy imparted in a CT cervical spine scan is slightly lowering the tube current for the CT cervical spine scan, e.g., by 5.8%; for a chest CT scan, an effective measure for reducing thyroid dose would be excluding the thyroid as much as possible from the exposed range. The poor efficacy of in-plane shielding is illustrated by the 26% dose reduction for the thyroid by shielding whereas a 46% dose reduction could, at last theoretically, be achieved by reducing the tube current to a level that would yield the same image quality, quantified as noise in the images, compared with quality of the shielded images.

The breast shield markedly reduces dose to the breasts (30%) and the lungs (15%) but at a substantial increase of noise in the shielded images and at the cost of mild beam-hardening artefacts. Without breast shielding, relatively modest image noise was observed in the scanned range containing the breasts; with breast shields, noise became dominant in this—for diagnosis, most relevant—range compared with the adjacent imaged range within the lungs but outside the shielded range. Breast shielding reduced total energy imparted during the CT chest scan by 10.3%, a slightly higher noise level, i.e., 5.5% higher but for the radiologist still unnoticeable, and this would result if tube current have been reduced by the same percentage (Fig. 2b).

Theoretically, reduction of tube current by 30% could be implemented as an alternative to bismuth shielding to achieve an equal dose reduction for breast tissue during an unshielded chest scan while yielding better image quality compared with shielded acquisition. This is because the associated increased image noise at a 30% reduction of tube current remains well below noise observed within the shielded acquisition, except for the diagnostically less relevant shoulder region where the noise just reaches a level comparable with noise within the shielded range (Fig. 2b).

An intuitive argument further supports the observed limitations of selective shielding. It should be considered that dose reduction by selective shielding of eye lens, thyroid, or breasts is only achieved when the rotating X-ray tube reaches an anterior position relative to the supine patient. However, when the X-ray tube reaches a posterior position relative to the supine patient, the effect of the

selective shielding turns into a disadvantage that was not considered in previous studies. In the posterior position, transmission profiles generated by the X-ray beam that could contribute to image formation are partly attenuated by the shield, thus reducing the intensity of the useful signal available for image reconstruction.

Dose reduction observed in this study from shielding the eye lens, thyroid, and breast ranges from 27% to 30%. This is significantly lower than the reported reduction of 40–67% for adults in other studies. This might be explained by the applied method for assessment of tissue and organ dose in this study, which is probably more accurate than measurements performed on the skin.

Equivalent doses calculated for clinical acquisitions at our institute provided a rough frame of reference but wide variations from these values occur mainly because of variations in acquisition protocols between institutes. The values confirm that equivalent dose to the eye lens is well below the threshold dose for induction of cataract; dose to the breasts is of the same order of magnitude as in mammography.

The scope of this study is limited in a sense that the phantom only represents an average sized patient and not, for example, an obese patient or pediatric patients. The study did not consider acquisitions based on attenuation-based techniques for automatic exposure control or tube modulation. Such systems are now becoming available [18, 19] and are not compatible with selective shielding. In contrast to the effect of selective shielding, systems for automatic exposure control might contribute to a better balance between image quality and patient dose compared with the standard acquisition.

In conclusion, the application of in-plane selective shielding is discouraged for achieving radiation protection in CT brain, CT cervical spine, and CT chest scans of adults.

References

1. Brnic Z, Vekic B, Hebrang A, Anic P (2003) Efficacy of breast shielding during CT of the head. Eur Radiol 13(11):2436–2440
2. Beaconsfield T, Nicholson R, Thornton A, Al Kutoubi A (1998) Would thyroid and breast shielding be beneficial in CT of the head? Eur Radiol 8(4):664–667
3. Fricke BL, Donnelly LF, Frush DP, Yoshizumi T, Varchena V, Poe SA, Lucaya J (2003) In-plane bismuth breast shields for pediatric CT: effects on radiation dose and image quality using experimental and clinical data. AJR Am J Roentgenol 180(2):407–411
4. Hein E, Rogalla P, Klingebiel R, Hamm B (2002) Low-dose CT of the paranasal sinuses with eye lens protection: effect on image quality and radiation dose. Eur Radiol 12(7):1693–1696
5. Hopper KD, King SH, Lobell ME, TenHave TR, Weaver JS (1997) The breast: in-plane X-ray protection during diagnostic thoracic CT—shielding with bismuth radioprotective garments. Radiology 205(3):853–858
6. Hopper KD, Neuman JD, King SH, Kunselman AR (2001) Radioprotection to the eye during CT scanning. AJNR Am J Neuroradiol 22(6):1194–1198
7. Hopper KD (2002) Orbital, thyroid and breast superficial radiation shielding for patients undergoing diagnostic CT. Semin Ultrasound CT MR 23(5): 423–427
8. McLaughlin DJ, Mooney RB (2004) Dose reduction to radiosensitive tissues in CT. Do commercially available shields meet the users' needs? Clin Radiol 59(5):446–450
9. Perisinakis K, Raissaki M, Theocharopoulos N, Damilakis J, Gourtsoyiannis N (2005) Reduction of eye lens radiation dose by orbital bismuth shielding in pediatric patients undergoing CT of the head: a Monte Carlo study. Med Phys 32(4): 1024–1030
10. Mukundan S, Frush DP, Yoshizumi T, Toncheva G, Nguyen G, Marcus J (2004) The use of a bismuth shield to decrease radiation dose to the eye in children: an anthropomorphic phantom study. RSNA2004. Report No.: SSC15–05
11. Shrimpton PC, Wall BF, Fisher ES (1981) The tissue-equivalence of the Alderson Rando anthropomorphic phantom for X-rays of diagnostic qualities. Phys Med Biol 26(1): 133–139
12. Ford RL, Nelson WR (1978) The EGS code system. Stanford Linear Accelerator Center. Report No.: Report SLAC–210
13. Nelson WR, Hirayama H, Rogers DWO (1985) The EGS code system. Stanford Linear Accelerator Center Report No.: Report SLAC–265
14. Salvado M, Lopez M, Morant JJ, Calzado A (2005) Monte Carlo calculation of radiation dose in CT examinations using phantom and patient tomographic models. Radiat Prot Dosimetry 114(1–3):364–368
15. van Straten M, Venema HW, Hartman J, den Heeten GJ, Grimbergen CA (2004) Reproducibility of multi-slice spiral computed tomography scans: an experimental study. Med Phys 31 (10):2785–2786
16. ICRP publication 60. 1990 (1991) Recommendations of the International Commission on Radiological Protection. Pergamon Press, Oxford
17. Tzedakis A, Damilakis J, Perisinakis K, Stratakis J, Gourtsoyiannis N (2005) The effect of z overscanning on patient effective dose from multidetector helical computed tomography examinations. Med Phys 32(6):1621–1629
18. Greess H, Wolf H, Baum U, Lell M, Pirkl M, Kalender W, Bautz WA (2000) Dose reduction in computed tomography by attenuation-based on-line modulation of tube current: evaluation of six anatomical regions. Eur Radiol 10(2):391–394
19. Mulkens TH, Bellinck P, Baeyaert M, Ghysen D, Van Dijck X, Mussen E, Venstermans C, Termote JL (2005) Use of an automatic exposure control mechanism for dose optimization in multi-detector row CT examinations: clinical evaluation. Radiology 237 (1):213–223